Transparent liquid-crystal-based microlens array using vertically aligned carbon nanofiber electrodes on quartz substrates

Transparent liquid-crystal-based microlens array using vertically aligned carbon nanofiber electrodes on quartz substrates

Qing Dai, Ranjith Rajasekharan, Haider Butt, Kanghee Won, Xiaozhi Wang, Timothy D Wilkinson and Gehan Amaragtunga

Department of Engineering (Division B), Cape Building, University of Cambridge, 9 J J Thomson Avenue, Cambridge CB3 0FA, UK

E-mail: qd205@cam.ac.uk

Received 16 September 2010, in final form 15 November 2010
Published 4 February 2011
Online at stacks.iop.org/Nano/22/115201

Abstract
A novel transparent liquid-crystal-based microlens array has been fabricated using an array of vertically aligned multi-wall carbon nanofibers (MWCNFs) on a quartz substrate and its optical characteristics investigated. Electron beam lithography was used for the catalyst patterning on a quartz substrate to grow the MWCNF array of electrodes. The structure of the electrode array was determined through simulation to achieve the best optical performance. Both the patterned catalyst and growth parameters were optimized for optimal MWCNF properties. We report an in-depth optical characterization of these reconfigurable hybrid liquid crystal and nanofiber microlens arrays.

1. Introduction

Many nanophotonic and electronic devices can be constructed from arrays of multi-wall carbon nanofibers (MWCNFs) which are grown on optically transparent substrates such as quartz. Possible device applications include electron emitters for field emission displays (FEDs) [1], network transistors [2] for replacing thin film transistors (TFTs) in liquid crystal displays and nanoscale coaxial antennas which act as visible light waveguides [3]. We have recently demonstrated a novel liquid-crystal (LC)-based reconfigurable microlens array (MLA) [4], which operates in reflective mode utilizing MWCNFs grown on an opaque Si substrate as electrode structures. If a transparent substrate is used, this MLA can operate in transmissive mode, making it a more practical and efficient device which could be used in many applications such as optical sensors, wavefront sensing, diffusers and 3D displays. Several papers have been reported on single- and multi-wall nanotube growth on transparent substrates by thermal or plasma-enhanced chemical vapor deposition (PECVD) [5–8], but these tubes are mostly in forest form leading to limited field enhancement and are not useful for photonics as they are highly absorbing (black). Ren *et al* [9, 10] successfully grew vertically aligned CNTs on a glass substrate but these tubes were randomly aligned and are not suitable for our proposed photonic devices, which require a periodic arrangement of the nanofiber electrodes. There are also groups who have reported fabrication of vertically aligned MWCNFs on silicon substrates and metallic substrates [11–16]. However, these substrates are all opaque.

In this paper, we demonstrate a novel transparent reconfigurable liquid crystal microlens array utilizing arrays of vertically aligned multi-wall carbon nanofibers (MWCNFs) as electrodes. We report the fabrication of the patterned vertically aligned carbon nanofiber array on a quartz substrate using a plasma-enhanced chemical vapor deposition process. By optimizing the growth conditions, we have also improved the morphology of the MWCNF array which allows the final device to achieve better optical performance in lensing when compared to the previous devices fabricated on silicon substrates. We have also studied the optical characteristics of these devices to prove that they behave as a reconfigurable microlens arrays.

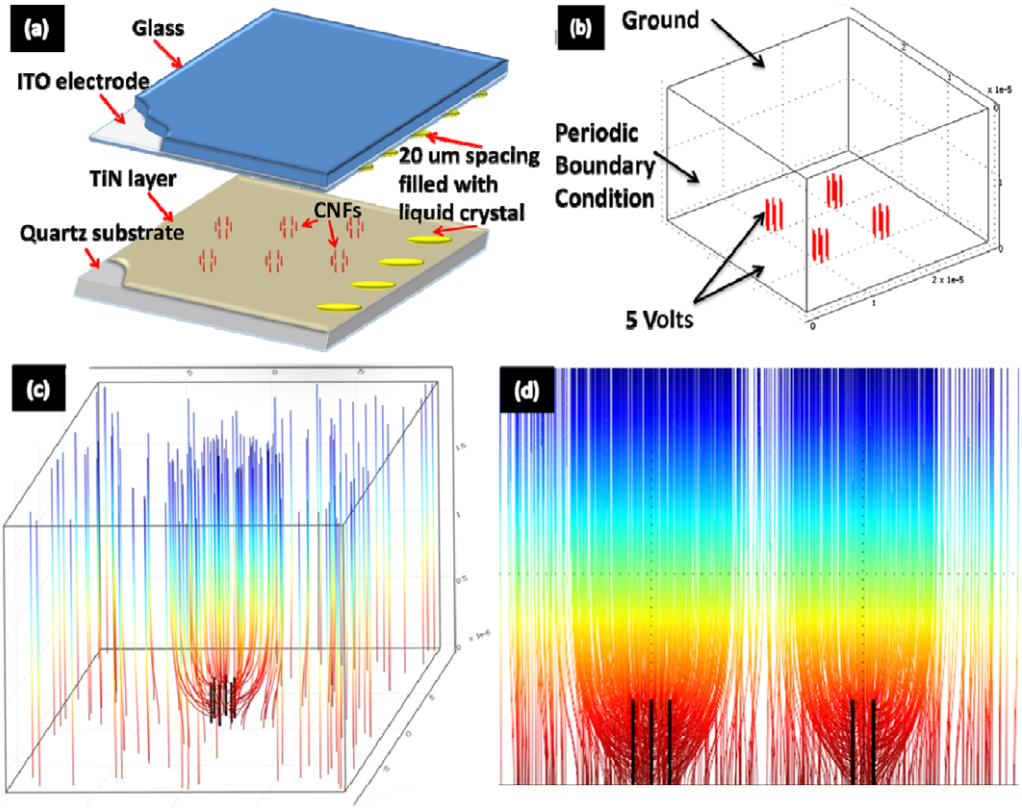

Figure 1. (a) The schematic diagram of the LC-based MLA using MWCNFs as electrodes. (b) The simulated 3D model of the device with the specified boundary conditions. The electric field generated by the MWCNF electrodes is simulated (in vacuum). (c) 3D electrostatic electric field profile produced by the six CNFs array. (b) 2D view of the Gaussian electric field profiles from hexagonal pattern (left) compared with square pattern of 4 CNFs (right).

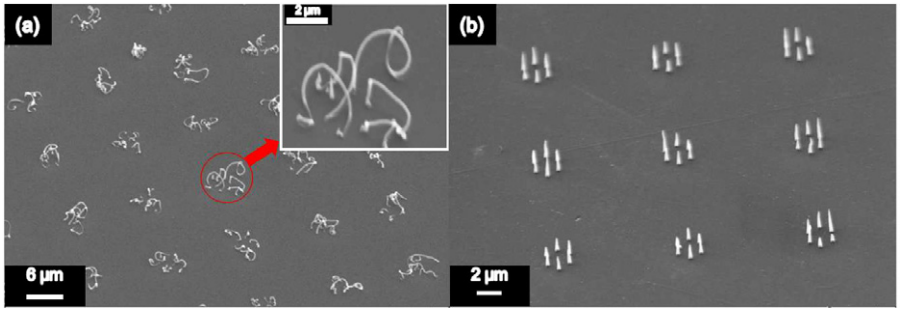

Figure 2. Synthesized CNFs: (a) on the plain quartz substrate and (b) on the quartz substrate coated with TiN thin film.

2. Simulation

The working principle of the microlens array is to align the LC molecules into a lens-like graded index structure using the Gaussian electric field profile generated by the MWCNF electrodes when a voltage is applied to them. The incoming light is then focused/defocused, depending on the alignment of the LC molecules controlled by the applied voltage. The schematic diagram of the device is shown in figure 1(a). The lower electrode consists of the MWCNFs on a quartz substrate (with TiN sputtered to connect the MWCNFs) and the top electrode of ITO-coated glass. The performance of the microlens arrays is greatly dependent on the electric field generated from the MWCNF electrodes. Due to field shielding effects (which reduce field enhancement from adjacent nanofibers), individual CNFs are preferred rather than a forest [17–19]. To obtain the optimized electrode geometry we investigated a number of CNF geometries to produce the strongest electric fields using the finite-element-method-based COMSOL Multiphysics simulation software. The MWCNF device model simulated is shown in figure 1(b). The boundary condition of the lower electrode (CNFs and lower plate) was set to a potential of 5 V_{rms} and the top electrode plate was set to 0 V. The lateral edges of the model were set to a periodic boundary condition to simulate the array. The resultant electric fields generated were studied for various CNF geometries. The

simulated electric field profiles generated by the CNFs were Gaussian in nature; they presented the highest electric field intensity in a region closest to the CNF tips and decreased further from it, as shown in figures 1(c)–(d). The simulated results, presented in more detail in [20], are in agreement with the experimental characterization of the CNFs field profile reported in [21]. It was found that the CNFs grown in hexagonal groups generated the strongest resultant electric fields having a wider overall Gaussian profiles, compared to the groups of one, two, three, four or five CNFs. Figure 1(d) shows the comparison of the Gaussian electric field profiles displayed by the hexagonal (6 CNFs) and square (4 CNFs) patterned groups and confirms that the hexagonal pattern produced a wider Gaussian electric field profile as required to make a microlens [4]. Also, the strength (intensity/amplitude) of the electric field decreased when more than six CNFs were used, due to field shielding effects.

Based on these simulation results, the devices were fabricated with the MWCNF electrodes grown in hexagonal groups, with each MWCNF having a 100 nm diameter and placed at a 1 μm spacing. These hexagonal groups were placed 10 μm from each other to form the electrodes for the microlens array.

3. Substrate preparation and MWCNF growth

To prepare the substrates, a titanium nitride (TiN) thin film was deposited on the quartz substrates, forming a transparent conductive layer. Next, an array of 100 nm diameter dots was patterned by electron beam lithography. Then a 20 nm indium tin oxide (ITO as diffusion barrier layer) and a 7 nm catalyst (Fe or Ni) thin film were sputtered sequentially before a lift-off process. The PECVD growth recipe is described as follows: the sample was heated up to 800 °C. Pre-treatment using NH_3 gas (200 sccm) was carried out for 60 s to anneal the catalyst. After that, the plasma was ignited by applying a voltage (640 V) between the grounded stage and the showerhead with an NH_3/C_2H_2 (200/50 sccm) gas mixture pumped in at a pressure of 3.1 mbar for 25–30 min. This gave rise to the MWCNF growth, allowing heights of around 3.5 μm. The amorphous carbon deposited during the CNF growth process was removed by post-treatment, placing the sample in a furnace heated to 500 °C for 30 min in air [22, 23].

3.1. Conductive layer for e-beam lithography and CNF growth

According to the simulation results, the morphology of the CNFs used as electrode devices must be vertically aligned while having a high aspect ratio, in order to generate strong electric fields for aligning the liquid crystal molecules. However, the CNFs did not grow vertically without the TiN thin film, as observed in figure 2(a). The reason for this is that the dc plasma cannot be sustained on a dielectric substrate and the CNFs were mostly grown due to thermal CVD. In the case having the TiN thin film, the sample surface was conductive and vertically aligned CNFs were synthesized as shown in figure 2(b).

3.2. Catalysts selection of CNF growth

The dependence of the catalyst on the morphology of the CNFs was also studied. Figure 3 shows SEM and AFM images of the grown MWCNFs using different catalysts. When Fe was selected as a catalyst, as shown in figure 3(a), multiple CNFs were synthesized on each catalyst dot. Single CNFs were obtained on each catalyst dot when an Ni catalyst was used, as shown in figure 3(b). CNFs typically have a diameter of 100–150 nm. Previous work demonstrates that, on silicon substrates, different catalysts captured the carbon feedstock for nanofiber nucleation, giving different CNF structures and diameters [24]. However, no similar experiments have been done previously on quartz substrates. We also investigated the post-annealing sizes of Fe and Ni catalyst dots using an atomic force microscope (AFM) and found that the Fe catalyst dot size was around 50 nm, which was smaller than the Ni dots ($\sim$100 nm) as shown in figures 3(c) and (d). This experiment confirms the morphologies of the grown CNFs using different catalysts. It shows that Ni is more suitable as a catalyst for CNF growth on quartz substrates compared to Fe. Our optical experiments also demonstrated that the electrodes grown with Ni catalyst had larger electric field enhancement, due to the single fiber at each catalyst dot location.

3.3. Growth parameter optimization

In order to increase the aspect ratio of the CNFs, we optimized annealing time and growth temperature for the quartz substrate. The annealing process was used to increase the catalyst surface roughness by breaking up the metal at certain temperatures to form submicron islands on the surface. However, due to the poor thermal conductivity of the quartz substrate, a 150 °C temperature difference was observed between the upper and lower surfaces during the heating process, which not only prevented an accurate growth temperature measurement but also made the catalyst annealing very difficult to control. Consequently, PECVD growth on a quartz substrate required a higher heating temperature and a longer annealing time than on an Si substrate.

In this experiment, the aspect ratios of the grown CNFs were measured under different annealing times and growth temperatures. According to figure 4(a), the highest aspect ratio was achieved by using 60 s annealing time and 800 °C growth temperature. As annealing 60 s at 850 °C, multiple CNFs were observed at each of the catalyst dots. These multiple CNFs could distort the required electric field profile so this annealing condition was abandoned. Figure 4(b) shows the synthesized CNFs using this optimized growth condition and the low resolution TEM images shown in figures 4(c) and (d) confirmed the fiber structure of the grown CNFs. It is obvious that the aspect ratio of the synthesized CNFs was greatly improved compared to previous growths.

4. Optical characterization of the device

4.1. The device under optical microscope

After the patterned growth of MWCNFs, the LC-based microlens array was fabricated as shown in figure 5(a).

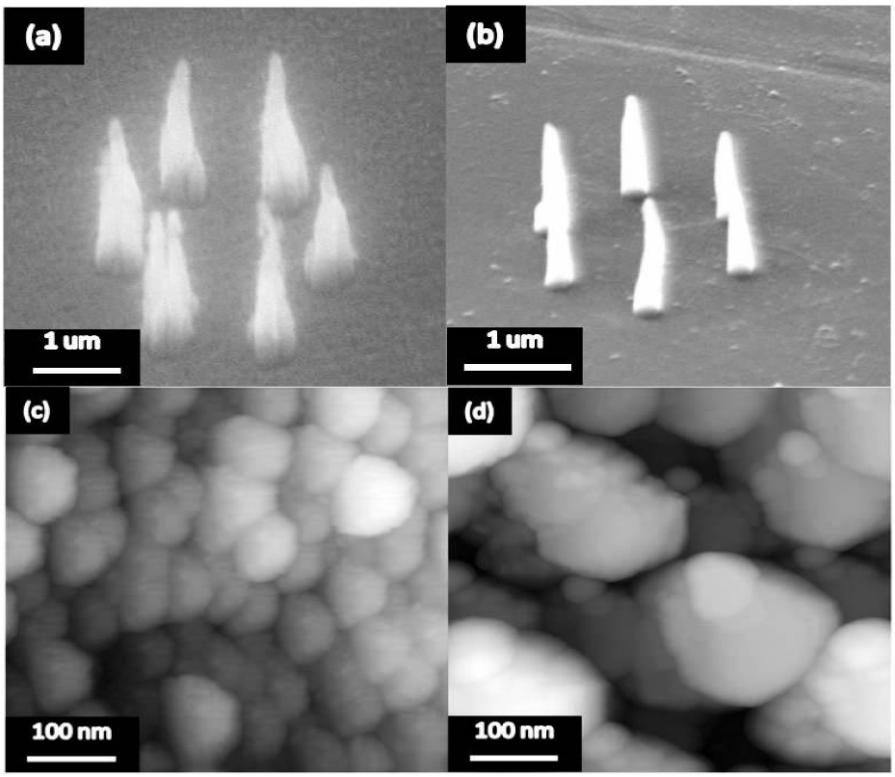

Figure 3. SEM images of CNFs using (a) Fe as catalyst and (b) Ni as catalyst. AFM images of catalysts after annealing with (c) Fe catalysts and (d) Ni catalysts.

The details of the device fabrication are discussed in [4]. The characteristics of the LC microlens array were studied using an Olympus optical microscope and its electro-optic parameters were measured with an HeNe laser (663 nm). Figure 5(b) shows the MLA with 0 V_{rms} applied voltage and the microscope adjusted to be out of focus. The image in figure 5(c) is the same area with an applied voltage of 2.1 V_{rms} with no adjustment made to the microscope. The image of nanofibers came into focus at such a voltage and hence the lensing function of the LC microlens was verified. The LC defect states were at the tips of the nanofibers and they came into focus as black dots at the center of each lenslet. The in-focus image was also brighter as the light now falls within the aperture of the microscope objective and was collected by the camera. Compared to previous devices which operated in the reflective mode [4], these microlens arrays on a transparent substrate have improved contrast ratio, as there is no double pass of light through the device.

4.2. Optical loss measurement

We also measured total optical losses from the device using an HeNe laser source, wavelength of 633 nm. A detector was used very near to the device on the other side to measure the transmission efficiency. The total optical loss was experimentally measured at 28% and the transmission measured at 72%. The reason for the optical losses are mainly due to the absorption of light by the nanofibers, scattering of light by the slightly deformed liquid crystal molecules around each nanofiber, absorption of light by the liquid crystal medium and titanium nitride (TiN) and ITO coating. The experiment was also repeated with white light.

4.3. Interference set-up to analyze the lens array

The lensing behavior of the device was experimentally verified using an interference-based set-up, using an optical microscope in transmission mode. A 633 nm wavelength laser was used as a light source and the device was mounted between a crossed polarizer and analyzer at an angle of 45°. Each six-nanotube group formed a lenslet and these lenslets were repeated with a 2D periodicity of 10 μm. The interference fringes were formed due to the interference between the ordinary and extraordinary beams being combined. The fringes were recorded on a CCD camera for further analysis. It was found that, in the absence of an external voltage, fringes were observed, which showed the alignment deformation of the liquid crystal molecules near the carbon nanotubes, even though the macroscopic alignment was planar. The interferogram of an array of lenslets at two different voltages is shown in figure 6. The fringes at each lenslet position became wider and better defined at 1.2 V_{rms}. As the voltage increased above 2.5 V_{rms}, the fringes started to disappear because the molecular alignment at each nanotube position became more homeotropic and hence less lensing was observed.

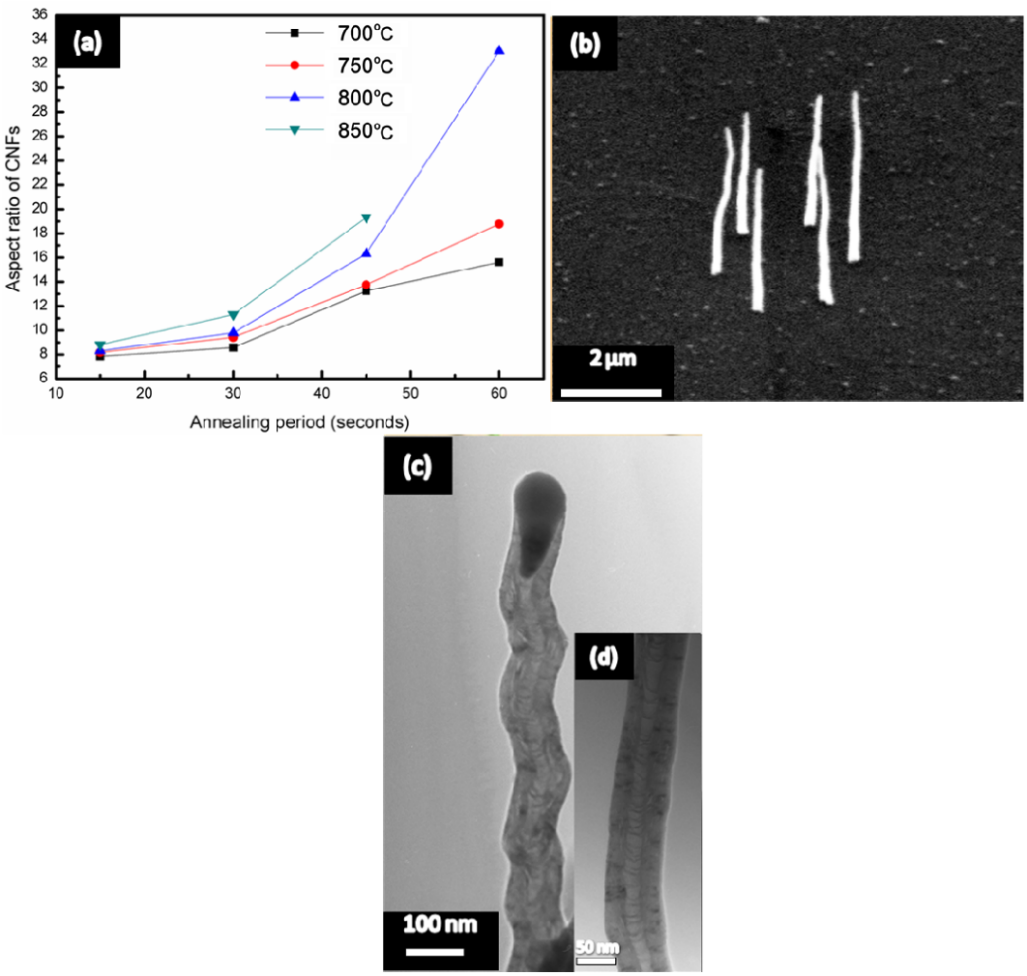

Figure 4. (a) Aspect ratios of CNFs as a function of the annealing times and grow temperatures, (b) synthesized CNFs after optimizing the growth recipe, (c) the low resolution TEM image of synthesized CNFs and (d) the low resolution TEM image to show its internal structure. (This figure is in colour only in the electronic version)

4.4. Phase profile of a lenslet

The interference fringes were further analyzed to study the optical phase profile of the lenslet. The recovery of the optical phase profile is very important in understanding the lensing properties and refractive index profile with respect to the applied voltage. A Fourier-transform-based technique was used to recover the phase profile from the fringes. We analyzed the wrapped phase profile of each lenslet at different voltages. The wrapped phase was unwrapped to get a continuous phase profile [25]. Figure 6(c) shows the unwrapped phase profile of a lenslet at 1.2 V_{rms}. The profile is roughly parabolic over each lenslet at 1.2 V_{rms}. The phase profile became distorted after 2 V_{rms}. The phase modulation was maximum at 1.2 V_{rms} with a value of 4π.

4.5. Focal length variation of a lenslet

We also obtained focal length variation of each lenslet with respect to voltage using the phase profile retrieved from the recorded interference fringes [25]. The phase profile of the device was dependent on the alignment of the liquid crystal in the device. A better LC alignment gives more phase modulation than a device with poor alignment. Figure 6(d) shows the focal length variation of samples with different alignment qualities. The focal length variation was from 11 to 15 μm for the voltage range 0–4 V_{rms} for a reflective device with poor alignment compared to 12–27 μm for a reflective device with good alignment. The focal length variation was from 10 to 34 μm for the transparent sample with good alignment. The focal length variation was better for the transparent sample because the light was incident normal to the device surface and there was no double pass through each microlenslet as in the case of the reflective device. It was also compatible with our simulation results as the redesigned electrodes, using the hexagonally patterned CNFs, generated a wider electric field profile. Only the transparent device can be easily used for imaging applications due to the ease of integration with the rest of the optical components and the reduced distortion in the image as there was no double pass. The focusing disappeared at higher voltages because of the vertical alignment of the liquid crystal [25–27]. Finally, the

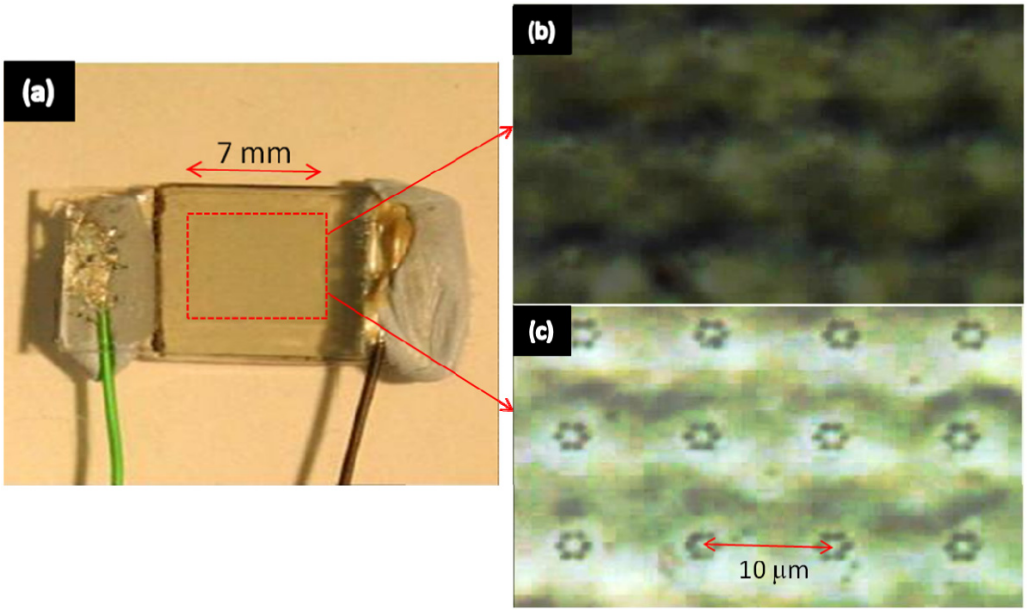

Figure 5. (a) The liquid-crystal (LC) and CNF-based microlens array (MLA) fabricated using a transparent indium tin oxide (ITO) electrode sputtered on the MWCNF substrate (CNF electrodes are in the red square area), (b) defocused area with 0 V_{rms} applied field and (c) the focused area with 2.1 V_{rms} applied field.

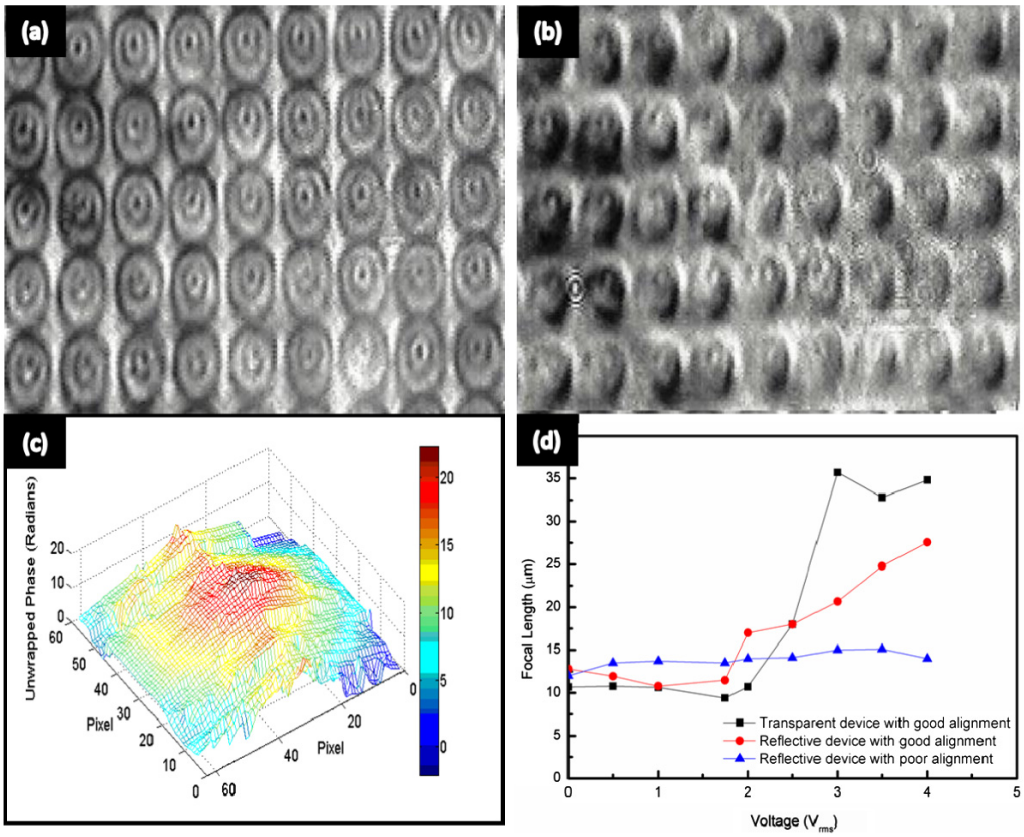

Figure 6. Interference fringes from an array of lenslets at two different voltages (a) 1.2 V_{rms} and (b) 2.5 V_{rms}. (c) Unwrapped phase profile of a lenslet at 1.2 V_{rms}. (d) The focal length variation of different devices as a function of the applied voltage.

optimized growth recipe enabled us to synthesize higher aspect ratio CNFs, which generated stronger field enhancement and controlled the liquid crystal molecules smoothly to form the desired Gaussian profile.

5. Conclusion

In conclusion, we have successfully fabricated transparent liquid crystal microlens arrays, using patterned vertically

aligned MWCNFs as electrodes on a quartz substrate. High aspect ratio MWCNFs were successfully grown using an optimized growth recipe for the PECVD process. We studied the lensing function of these microlens arrays and observed that their focal length was tuned by adjusting the applied voltage. According to the measurements, these transparent microlens arrays can achieve better optical performance, especially for imaging compared to reflective devices.

References

[1] Baughman R H, Zakhidov A A and de Heer W A 2002 *Science* **297** 787

[2] Snow E S, Novak J P, Campbell P M and Park D 2003 *Appl. Phys. Lett.* **82** 2145

[3] Rybczynski J, Kempa K, Herczynski A, Wang Y, Naughton M J and Ren Z F 2007 *Appl. Phys. Lett.* **90** 021104

[4] Wilkinson T D, Wang X Z, Teo K B K and Milne W I 2008 *Adv. Mater.* **20** 363–6

[5] Bae E J, Min Y-S, Kim U and Park W 2007 *Nanotechnology* **18** 015601

[6] Lee C J, Park J, Han S and Ihm J 2001 *Chem. Phys. Lett.* **337** 398

[7] Li Y J, Sun Z, Lau S P, Chen G Y and Tay B K 2001 *Appl. Phys. Lett.* **79** 1670

[8] Shiroishi T, Sawada T, Hosono A, Nakata S, Kanazawa Y and Takai M 2004 *J. Vac. Sci. Technol.* B **22** 1834

[9] Ren Z F, Huang Z P, Xu J W, Wang J H, Bush P, Siegal M P and Provencio P N 1998 *Science* **282** 1105

[10] Huang Z P, Carnahan D L, Rybczynski J, Giersig M, Sennett M, Wang D Z, Wen J G, Kempa K and Ren Z F 2003 *Appl. Phys. Lett.* **82** 460

[11] Suh J S S, Jeong K S, Lee J S and Han I 2002 *Appl. Phys. Lett.* **80** 2392

[12] Semet V, Binh V T, Vincent P, Guillot D, Teo K B K, Chhowalla M, Amaratunga G A J, Milne W I, Legagneux P and Pribat D 2002 *Appl. Phys. Lett.* **81** 343

[13] Teo K B K, Chhowalla M, Amaratunga G A J, Milne W I, Priro G, Legagneux P, yczisk F, Pribat D and Hasko D G 2002 *Appl. Phys. Lett.* **80** 11–20

[14] Kim D H *et al* 2003 *Nanotechnology* **14** 1269–71

[15] Teo K B K *et al* 2003 *Nanotechnology* **14** 204

[16] Mauger M, Binh V T, Levesque A and Guillot D 2004 *Appl. Phys. Lett.* **85** 305

[17] Chhowalla M, Teo K B K, Ducati C, Rupesinghe N L, Amaratunga G A J, Ferrari A C, Roy D, Robertson J and Milne I W 2001 *J. Appl. Phys.* **90** 5308

[18] Nilsson L, Groening O, Emmenegger C, Kuettel O, Schaller E, Schlapbach L, Kind H, Bonard J M and Kern K 2000 *Appl. Phys. Lett.* **76** 2071

[19] Bonard J M, Weiss N, Kind H, Stockli T, Forro L, Kern K and Chatelain A 2001 *Adv. Mater.* **13** 184

[20] Butt H, Ranjith R, Wilkinson T D and Amaratunga G A J 2010 *IEEE Trans. Nanotechnol.* **99** 1

[21] Milne W I *et al* 2003 *Diamond Relat. Mater.* **12** 422–8

[22] Hou P, Liu C, Tong Y, Xu T, Liu M and Cheng M 2001 *J. Mater. Res.* **16** 9

[23] Collins P G, Bradley K, Ishigami M and Zettl A 2000 *Science* **287** 5459

[24] Robertson J 2007 *Mater. Today* **10** 36–43

[25] Rajesekharan R, Butt H and Wilkinson T D 2009 *Opt. Lett.* **34** 1237–9

[26] Rajesekharan R, Dai Q and Wilkinson T D 2010 *Appl. Opt.* **49** 2099–104

[27] Rajasekharan R, Bay C, Dai Q, Freeman J and Wilkinson T D 2010 *Appl. Phys. Lett.* **96** 233108